Numerical Analysis of Driver Thoracolumbar Spine Response in Frontal Crash Reconstruction

Xin Ye[1,2], Derek Jones[1,2], James Gaewsky[1,2], Logan Miller[1,2],
Joel Stitzel[1,2], Ashley Weaver[1,2]

[1] Wake Forest University School of Medicine; [2] Virginia Tech -Wake Forest University Center for Injury Biomechanics

ABSTRACT

This study aimed to reconstruct 11 motor vehicle crashes (six with thoracolumbar fractures and five without thoracolumbar fractures), and analyze the fracture mechanism, fracture pattern, associated vehicle parameters and driver attributes affecting fracture risk. Eleven frontal crashes were reconstructed with a finite element simplified vehicle model (SVM). The SVM was tuned to each case vehicle and the Total HUman Model for Safety (THUMS) v4.01 was scaled and positioned in a baseline configuration to mimic the pre-crash driver posture. For the six thoracolumbar fracture cases, 120 simulations to quantify uncertainty and variation were performed using a Latin Hypercube Design of Experiments (DOE) to vary: seat track position, seatback angle, steering column angle, steering column position, and D-ring height. Vertebral loads and bending moments were analyzed. Maximum principal strain and stress were collected in the vertebral cortical and trabecular bone. DOE data were fit to regression models to examine occupant positioning and thoracolumbar response correlations. Of the 11 cases, both the vertebral compression force and bending moment progressively increased from superior to inferior vertebrae. Two thoracic spine fracture cases had higher compression force and bending moment across all thoracic vertebral levels, compared to nine cases without thoracic spine fractures (force: 1200.6 vs. 640.8 N; moment: 13.7 vs. 9.2 Nm). While there was no apparent difference in bending moment at the L1-L2 vertebrae, lumbar fracture cases exhibited higher vertebral bending moments in L3-L4 (fracture/non-fracture: 45.7 vs. 33.8 Nm). A rearward seat track position and reclined seatback increased the thoracic spine bending moment by 111-329%. A more reclined seatback increased the lumbar force and bending moment by 16-165% and 67-172%, respectively. This study provided a computational framework for assessing thoracolumbar fractures, and also quantified the effect of pre-crash driver posture on fracture risk. Results aid in the understanding of factors contributing to thoracolumbar fractures.

INTRODUCTION

Despite recent advancement in vehicle crashworthiness, thoracic and lumbar spine fractures remain a problem. The incidence of thoracolumbar fractures in frontal crashes has increased as a function of vehicle model year from 1986 to 2008 in National Automotive Sampling System-Crashworthiness Data System (NASS-CDS) (Pintar et al. 2012). Other analyses of NASS-CDS, the National Trauma Databank (NTDB) and National Inpatient Sample (NIS) have shown thoracolumbar spine injury incidence increased over time when adjusting for

age (Doud et al. 2015). Similarly, vertebral fracture incidence increased in motor vehicle crashes (MVCs) from 1994 to 2002 in Crash Outcome Data Evaluation System data, despite the concomitant increase in seatbelt and airbag use (Wang et al. 2009). Analysis of 1996-2011 Crash Injury Research and Engineering Network (CIREN) data demonstrated an increasing incidence of thoracolumbar fractures with age and seatbelt use (Rao et al. 2014).

While compressive loading and bending moment were believed to be the predominant injury mechanism for thoracolumbar fractures, there is no established injury assessment for thoracolumbar fractures in MVC standards throughout the world (Stemper et al. 2015, Yoganandan et al. 2013). Countermeasures, including seatbelts and airbags, are effective in reducing MVC fatalities and injury severity, but they may not fully protect the thoracolumbar spine (Pintar et al. 2012, Rao et al. 2014).

The Total HUman Model for Safety (THUMS) finite element (FE) full human body model has been used to computationally simulate occupant response in side and frontal impact scenarios (Danelson et al. 2015, Gaewsky et al. 2015, Golman, Danelson and Stitzel 2015, Iwamoto, Nakahira and Kimpara 2015, Jones et al. 2016b, Ye et al. 2018). Previous studies used computational models to analyze driver kinematics and lower thoracic spine injury in racing cars during frontal impacts (Katsuhara et al. 2017). The biomechanics of lumbar spine motion and stiffness has also been characterized in frontal crash simulations (Arun et al. 2017). However, there is a lack of existing injury criteria to quantify the severity of thoracolumbar fractures, and few studies have examined the contributing factors, including driver posture and vehicle attributes, on thoracolumbar fracture outcomes.

The aim of this study was to evaluate thoracolumbar fractures from FE reconstruction of MVCs, and to examine factors affecting fracture risk. It is hypothesized that force and moment data derived from simulations could quantify thoracolumbar fracture severity and reflect the fracture incidence.

METHODS

CIREN/NASS-CDS Case Selection

Eleven full-frontal crashes were selected for FE reconstruction from the NASS-CDS and CIREN databases (Table 1). Each frontal planar MVC case had a Collision Deformation Classification (CDC) code of “FDEW” and a principal direction of force (PDOF) between 350° and 10°. All cases involved belted drivers and vehicle model years of 2002 and later. Crashes with frontal airbag deployment and an event data recorder (EDR)-measured longitudinal Delta-V between 30-72 km/h were selected for similar severity to regulatory crash tests. Of the 11 selected cases, six cases had one or more Abbreviated Injury Scale (AIS) 2 + thoracolumbar fractures. Injury information for each of the six cases with thoracolumbar fractures, including computed tomography (CT) scans and BioTab records documenting injury mechanisms, were collected and analyzed (Schneider et al. 2011). The injury mechanism of each fracture was also reviewed by an orthopaedic surgeon, and compared with the crash reconstruction results.

Table 1. Vehicle information and driver characteristics for 11 reconstructed cases

Case Vehicle	Source	Case ID	PDOF (°)	Delta-V (km/h)	Age	Sex	Mass (kg)	Height (cm)	Vertebrae Fractured
2002 Chevrolet Cavalier	NASS	126015217	0	49.4	18	M	64	175	–
2010 Toyota Camry	CIREN	338103538	10	64.0	21	F	64	160	–
2005 Chevrolet Silverado	NASS	437010451	0	59.9	23	M	79	175	T12, L1
2008 Lexus ES350	CIREN	317349598	10	69.7	43	M	88	175	–
2007 Hummer H3	NASS	784014636	350	57.4	50	F	86	173	–
2007 Toyota Solara	CIREN	588557622	350	31.8	50	F	67	173	T1-T6, T8, L1, L2
2007 Toyota Corolla	CIREN	431354202	350	54.5	57	M	71	165	L4
2012 Honda Civic	CIREN	359501964	0	56.3	67	F	66	165	–
2006 Chevrolet Malibu	CIREN	128763	350	61.1	69	M	82	173	L1, L2
2006 Chevrolet Cobalt	CIREN	385119464	350	42.6	80	M	77	183	L1, L3
2012 Ford Escape	CIREN	359544180	0	49.9	86	M	84	175	L3

Case Reconstruction

A semi-automated procedure was developed for FE crash reconstruction in a simplified vehicle model (SVM). The SVM was previously developed as an aggregate of laser scans from 14 different vehicle interiors, and represented a generic vehicle geometry profile (Iraeus and Lindquist 2016). The SVM was updated to include several restraint systems, including a seatbelt with pre-tensioner and load-limiting retractor, frontal airbag and knee airbag (Jones et al. 2016a, Ye et al. 2016). The SVM was tuned in each case reconstruction to simulate a specific vehicle model using a previously published approach (Ye et al. 2018). Briefly, a Hybrid III 50th percentile model (Humanetics, Plymouth, MI) was positioned in the SVM according to anthropometric measurements from a frontal New Car Assessment Program (NCAP) test of the particular vehicle model. A Latin Hypercube Design of Experiments (DOE) was performed for each case to optimize the SVM structural properties to mimic vehicle-specific response. The vehicle parameters yielding the most similar crash response, according to a Sprague and Geers analysis, were then used to tune the SVM to represent the specific vehicle model in subsequent crash simulations with the THUMS model (Jones et al. 2016a, Ye et al. 2016).

THUMS Modeling

Isometric scaling was applied to the THUMS v4.01 model using a combination of height and mass scaling factors to minimize the error between THUMS and case-specific driver anthropometry (Eqn 1-3) (Miller et al. 2016). The scale factor in Eqn 3 was used to scale the THUMS length in the X, Y, and Z dimensions simultaneously.

$$height\ factor = \frac{case\ occupant\ height}{THUMS\ model\ height} \quad \text{Eqn1}$$

$$mass\ factor = \sqrt[3]{\frac{case\ occupant\ mass}{THUMS\ model\ mass}} \quad \text{Eqn2}$$

$$scale\ factor = \frac{height\ factor + mass\ factor}{2} \quad \text{Eqn3}$$

The THUMS was gravitationally settled in the global-Z direction, and positioned in the baseline posture, based on the longitudinal seat track position, seatback angle, D-ring anchor height, steering column position and steering column angle recorded in NASS-CDS or CIREN. For the six thoracolumbar fracture cases, these five parameters were varied using a Latin Hypercube DOE to investigate the pre-crash driving posture effect on thoracolumbar fracture risk (Table 2). In the DOE, 120 simulations were conducted to quantify uncertainty and response variation for each case, with the range of each occupant positioning parameter identified from frontal NCAP crash test reports of comparable vehicle models, based on the vehicle year and model interchange list (Anderson 2004). For each of the baseline cases and associated DOEs with the positioned THUMS, the EDR crash pulse from the CIREN or NASS-CDS case was applied to the SVM.

Table 2. Occupant positioning parameters for 11 reconstructed cases. Intervals indicate the range for the corresponding DOE for cases with thoracolumbar fractures

Case	Seat Track Position (mm)		Seatback Angle (°)		D-Ring Height (mm)		Steering Column Position (mm)		Steering Column Angle (°)	
Cavalier	120		15		0		0		24	
Camry	0		12		0		0		5	
Silverado	0	[-50,75]	12	[0,35]	NA		0	[-10,10]	21	[11.3,36.7]
Lexus	100		15		75		0		25	
Hummer	10		15		50		0		9.7	
Solara	-80	[-120,25]	5	[-3,25]	25	[0,75]	0	[-22.5,22]	25	[17.2,33.3]
Corolla	-75	[-40,125]	10	[-5,35]	25	[-10,85]	25	[-30,30]	29.1	[25.5,29.1]
Civic	0		10		75		0		24	
Malibu	0	[-75,75]	16	[0,35]	0	[0,100]	0	[-26,26]	23	[20.7,25]
Cobalt	65	[-40,130]	12	[0,33]	75	[0,100]	0	[-30,30]	20	[18,22]
Escape	65	[-40,130]	12	[0,33]	75	[0,100]	0	[-30,30]	20	[18,22]

Data Analysis

Virtual accelerometers were implemented in the THUMS model at the T1, T6, T9 and T12 vertebrae using *CONSTRAINED_INTERPOLATION. This allows for measurement of six

degrees of freedom accelerations at regional levels of the selected vertebrae. Additionally, load cells were modeled at each level of the thoracic and lumbar vertebrae using *DATABASE_CROSS_SECTION to measure load in elements of each mid-vertebral cross-section (Figure 1).

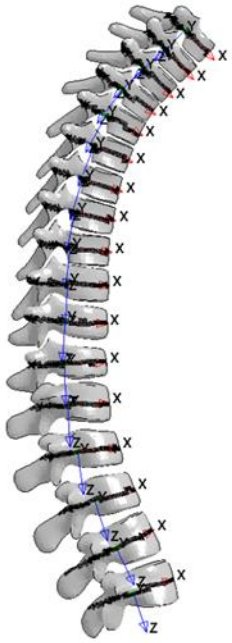

Figure 1. THUMS thoracolumbar local coordinate systems and cross-section instrumentation.

The cross sections, positioned transversely through the center of gravity of each vertebral body, output forces and moments in their respective local coordinate systems. These local coordinate systems were aligned to their corresponding vertebral body cross-sections using *CONSTRAINED_NODAL_RIGID_BODY, with the positive Z direction pointing downward, and positive X forward following the SAE J211 sign convention (SAE 2007). Stress and strain data for the cortical and trabecular bone of the thoracic and lumbar spine, including maximum principal stress and maximum principal strain, were also measured.

RESULTS

Baseline Cases

Two cases resulted in thoracic spine fractures: 1) the Solara occupant sustained compression fractures in the T1-T4, T6, and T8 vertebrae, and a T5 spinous process fracture; 2) the Silverado occupant sustained a T12 compression fracture. Solara simulations indicated an average compression force of 635.2 N in T1-T4, and an average compression force of 1290.5 N in T5-T8, which was the highest of all 11 reconstructed cases. Both the Silverado and Solara occupants sustained elevated compression forces of 1829.5 and 2057.9 N at T12, respectively, higher than the other nine cases. In terms of thoracic bending moment, the peak flexion bending moment was categorized into three groups by anatomical thoracic regions: upper (T1-T4),

middle (T5-T8), and lower (T9-T12). On average, the two cases with thoracic spine fractures sustained higher bending moments at all three thoracic spine levels (upper: 14.5, middle: 14.0, lower: 12.7 Nm), compared to the nine cases without thoracic spine fractures (upper: 8.5, middle: 7.1, lower: 12.1 Nm).

Six case occupants sustained lumbar spine fractures: Cobalt (L1, L3), Corolla (L4), Escape (L3), Malibu (L1, L2), Silverado (L1), and Solara (L1, L2). Both the lumbar compression force and bending moment progressively increased from superior to inferior vertebral level, regardless of fracture outcome. On average, the six occupants with lumbar spine fractures had higher compression forces (L1-L3: 1359.0, L4-L5: 1782.6 N) than occupants without lumbar spine fracture (L1-L3: 1198.1, L4-L5: 1596.5 N). Two cases with the highest average L1-L4 compression force (Silverado and Solara) resulted in lumbar spine fractures, while the majority of lumbar spine fractures occurred in older occupants, suggesting that age maybe a contributor to increased fracture risk (Figure 2). Additionally, the distinction between fractured and non-fractured cases was more noticeable at each individual lumbar spine vertebral level (Figure A1, Appendix). All occupants with L1 spine fractures had relative high compression forces in the L1 vertebra, with the Solara occupant having the highest compression force (2083.8 N). The Solara occupant also had the highest L2 compression force of 2112.5 N. The L3 compression forces were in the mid-range for the Escape and Cobalt occupants. While these two cases involved occupants with oldest age, the bending moments in these two occupants were also elevated in comparison to occupants without L3 fractures (Figure A2, Appendix).

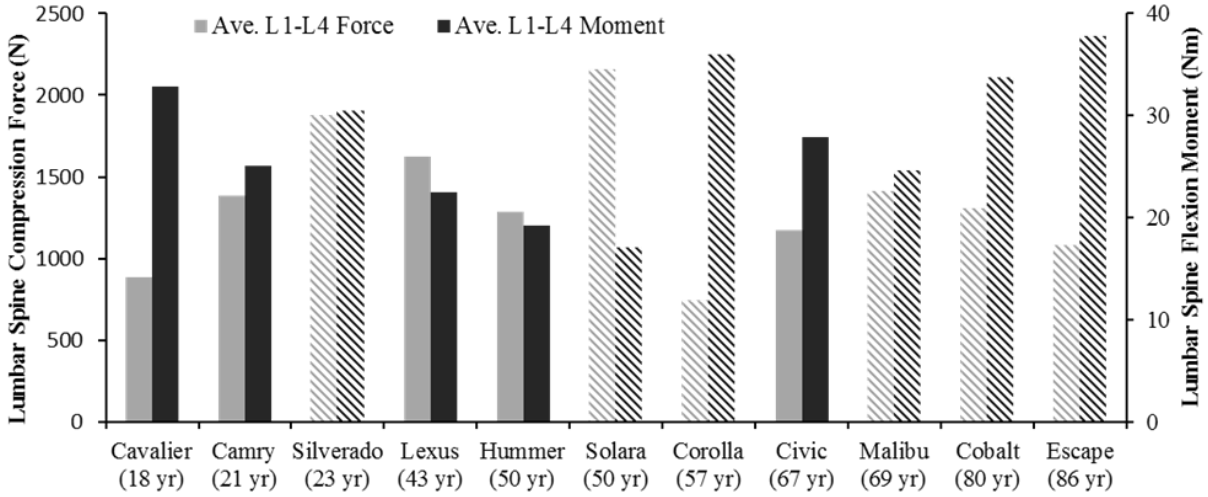

Figure 2. Average lumbar spine L1-L4 compression force and flexion moment of 11 reconstructed cases. Hatched bars indicated lumbar spine fractures.

The average bending moment for occupants with lumbar spine fractures (L1-L3: 23.7, L4-L5: 60.0 Nm) was also slightly higher than occupants without lumbar spine fractures (L1-L3: 19.8, L4-L5, 52.7 Nm). There was no apparent difference in bending moment magnitude between fracture and non-fracture cases for the L1 and L2 vertebrae, while fracture cases sustained higher vertebral bending moments in the L3 and L4 vertebrae (Figure A2, Appendix). The Malibu case sustained a relatively low bending moment, suggesting compression force may be the dominant injury mechanism for the L1 and L2 fractures sustained by this occupant, and age (69 years) could be a contributing factor. The Escape and Cobalt occupants sustained L3 compression fractures, which corresponded to the first and second highest bending moments of

44.5 and 34.1 Nm, respectively. Similarly, the Corolla occupant had a L4 endplate fracture, which was reflected by a 54.4 Nm (third highest in magnitude) L4 bending moment. In contrary to the high axial compression force, both the Silverado (15.1, 17.7 Nm) and Solara (12.6, 14.6 Nm) occupants had lower bending moments at the L1 and L2 vertebral levels.

The maximum principal strain for both the trabecular and cortical bone of each vertebra was calculated (Figures 3). On average, the six occupants with thoracolumbar fractures sustained higher strain in the trabecular bone (T12: 1.70%, L1-L3: 1.64%, L4-L5: 1.59%), compared to five occupants without thoracolumbar fractures (T12: 1.51%, L1-L3: 1.20%, L4-L5: 1.33%). The Silverado occupant sustained the highest average principal strain of 2.52% across L1-L5, followed by Corolla (2.31%) and Solara (2.15%), which all sustained thoracolumbar fractures.

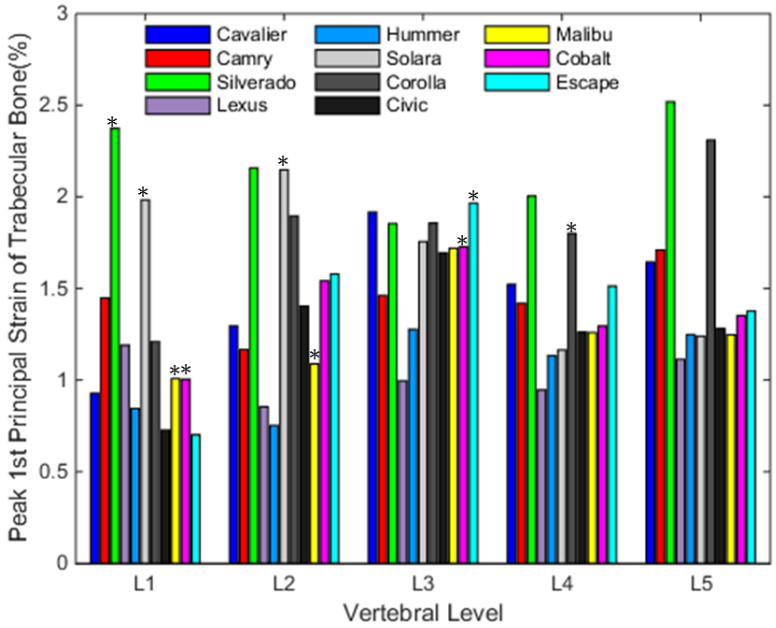

Figure 3. Maximum principal strain of trabecular bone in the vertebrae. Asterisks indicate lumbar spine fractures.

The maximum principal strains of vertebral cortex were generally lower than the trabecular bone. Similar trends were observed in terms of relative ranking in maximum principal strain magnitude in the cortex among the 11 occupants. Additionally, the maximum principal strain of the cortical bone proved to be a good indicator of fracture occurrence across the T12 to L5 vertebrae, with higher strain values in vertebral levels with fractures (Figure 4).

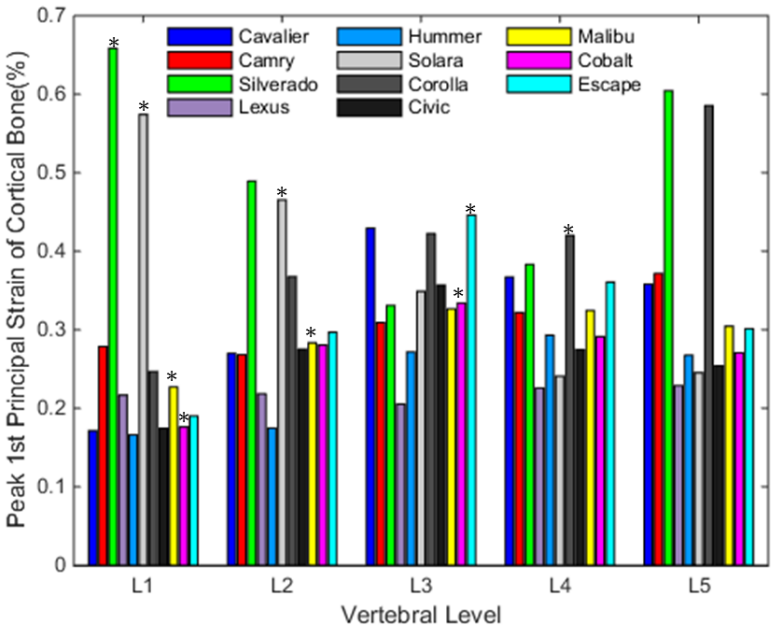

Figure 4. Maximum principal strain of cortical bone in the vertebrae. Asterisks indicate lumbar spine fractures.

The maximum principal stress for trabecular and cortical bone of the vertebrae was also calculated (Figures 5-6). Occupants with thoracolumbar fractures had higher maximum principal stress in the trabecular bone (T12: 1.9, L1-L3: 1.2, L4-L5: 1.1 MPa), compared to occupants without thoracolumbar fracture (T12: 1.7, L1-L3: 1.0, L4-L5: 0.9 MPa). While the maximum principal stress of cortical bone was much higher than the trabecular bone, on average occupants with fracture (T12: 70.7, L1-L3: 68.6, L4-L5: 100.6 MPa) also sustained a higher peak principal stress than occupants without fracture (T12: 45.2, L1-L3: 45.7, L4-L5: 91.1 MPa).

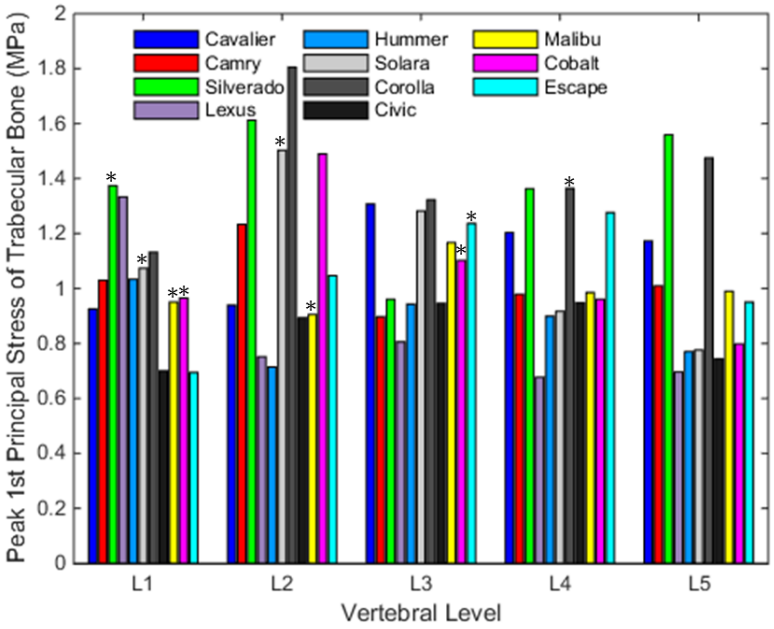

Figure 5. Maximum principal stress of trabecular bone in the vertebrae. Asterisks indicate lumbar spine fractures.

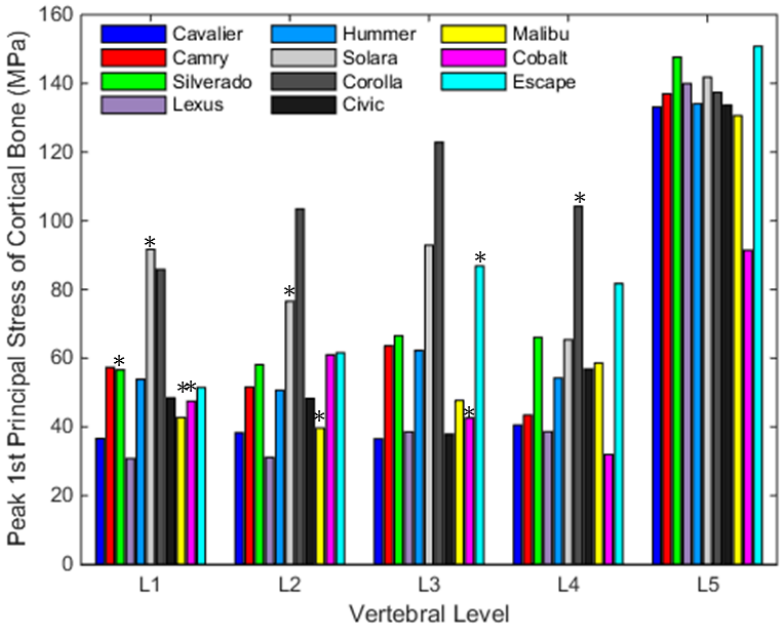

Figure 6. Maximum principal stress of cortical bone in the vertebrae. Asterisks indicate lumbar spine fractures.

Parametric Study

For each of the six cases with thoracolumbar fractures, regression analysis was performed on the 120 simulations with varied driver posture to examine any relationship between occupant position and thoracolumbar spine response. This parametric study was performed in a full-factorial DOE fashion to examine any combination with occupant position parameters as independent variables and the spine measurements as dependent variables. Adjusted R-squared values were used to quantify the goodness of fit for each linear regression model.

Seat track position and seatback angle strongly affected spine response (R^2_{adj} >0.50), while D-ring anchor height, steering column position and steering column angle had negligible effects. For thoracolumbar fracture cases, a rearward seat track and more reclined seatback increased the thoracic bending moment by 111-329%. A more reclined seatback also increased the lumbar force and bending moment by 16-165% and 67-172%, respectively. For instance, the Corolla occupant's L4 bending moment increased by 66.9 Nm with a seatback angle change of 35 degrees (Figure 7). The Silverado occupant's T12 bending moment increased by 14.5 Nm when translating the seat track from forward to rearward by 140 mm.

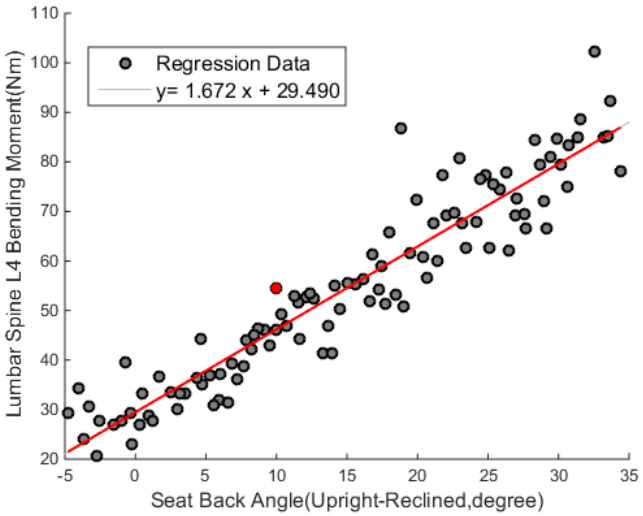

Figure 7. Linear regression fit of L4 flexion moment versus seatback angle for the Corolla case. Red circle indicates the baseline occupant posture.

DISCUSSION

This study combined real-world crash information and computational models to reconstruct 11 MVCs. Reconstructed cases with thoracolumbar fractures generally demonstrated higher axial compression forces or flexion bending moments. Previous studies regarding the injury risk of spinal injuries were limited by boundary conditions and sample size. One study performed drop-tower tests from cadaveric vertebrae, and indicated that a peak force of 3.4 kN corresponds to 50% fracture risk for the upper and lower thoracic spine, while a peak force of 3.7 kN corresponds to 50% fracture risk with thoracic and lumbar spine combined (Yoganandan et al. 2013). While the majority of the cases fell into a fracture risk below 10% based on this injury risk function, it should be noted that this injury risk function only considered axial compression with a static initial condition, while the contribution of bending moment and moment inertia were not considered.

Stress and strain data were also measured at trabecular and cortical regions of each vertebra. One study examined compression properties of lumbar trabecular bone, and found a yield and ultimate strain of 6.0 ± 2.2% and 7.4 ± 2.4% on average, respectively, as well as an ultimate stress of 1.55 ± 1.11 MPa (Hansson, Keller and Panjabi 1987). Another study examining the maximum principal stress and strain from T10 to L4 trabecular bone found an ultimate strain of 1.5-1.6% and an ultimate stress of 2.2 MPa (Kopperdahl and Keaveny 1998). A yield strain of 1.3-1.5% from thoracic vertebra cortex has also been reported (Kayanja, Ferrara and Lieberman 2004). Results from the current study fell into these ranges, and maximum principal strain proved to be a good indicator of fracture occurrence.

Results from the parametric study revealed that seatback angle and seat track position could affect the thoracolumbar spine response. Only 17% of drivers maintain the standard driving posture (Hault-Dubrulle et al. 2011, Morris, Cross and Bingley 2005), and current study quantifies thoracolumbar response variation for a wide range of driving postures using a DOE approach. A more reclined seatback angle and a rearward seat track position increased the thoracolumbar axial compression force as well as bending moment. This finding was consistent

with a previous study of crash reconstruction based on four MVCs (Jones et al. 2016b). Another study supported this finding, and found an increased mortality risk in both partially reclined (Odds Ratio, OR: 1.15; 95% Confidence Interval, CI: 1.05-1.26) and fully reclined (OR: 1.77; CI: 1.09-2.88) occupants (Dissanaike et al. 2008). Future studies could optimize seat design and position with an imminent crash to better protect the occupant from sustaining thoracolumbar fractures.

Several limitations exist in addition to those mentioned. First, occupant-specific bone quality was not considered in the crash reconstructions. Age is significantly associated with an increased risk of lumbar fractures, with each year in age increasing the odds of lumbar fracture by 4.0% (Kaufman et al. 2013). Several cases with thoracolumbar fractures involved older occupants, and the potential effect of osteopenia and osteoporosis was not considered at this juncture. Future studies could improve human body model biofidelity by incorporating morphing techniques and material property tuning to better represent specific occupants (Schoell et al. 2015, Vavalle et al. 2014, Zhang et al. 2017). Additionally, this study evaluated a limited sample of MVCs, and multiple confounding factors, including vehicle intrusions, seatbelt submarining, and pre-crash braking were not evaluated. Regardless, these crash reconstructions accurately estimated the increased axial force or bending moment of the thoracolumbar spine, and correlated well with the fracture occurrence.

CONCLUSIONS

In conclusion, 11 frontal MVCs, including six with thoracolumbar fractures, were selected from CIREN and NASS-CDS and reconstructed using a SVM and the THUMS FE model. This study developed a computational framework to assess thoracolumbar fractures based on kinetic and kinematic data, and elucidated the effect of pre-crash driver posture on thoracolumbar spine response using a parametric study. Results aid in the development of injury criteria to better quantify thoracolumbar injury severity, and the understanding of thoracolumbar fracture mechanisms and prevention.

ACKNOWLEDGEMENTS

Funding was provided by Toyota's Collaborative Safety Research Center. The authors thank the National Highway Traffic Safety Administration for support of the CIREN program and the WFU-VT CIREN Center (Cooperative Agreement DTN22-10-H-00294). Views expressed are those of the authors and do not represent the views of the sponsors.

REFERENCES

Anderson, G. (2004) Vehicle Year and Model Interchange List. *Scalia Safety Engineering*.

Arun, M. W., P. Hadagali, K. Driesslein, W. Curry, N. Yoganandan & F. A. Pintar (2017) Biomechanics of lumbar motion-segments in dynamic compression. *Stapp Car Crash J,* 61**,** 1-25.

Danelson, K. A., A. J. Golman, A. R. Kemper, F. S. Gayzik, H. Clay Gabler, S. M. Duma & J. D. Stitzel (2015) Finite element comparison of human and Hybrid III responses in a frontal impact. *Accident Analysis & Prevention,* 85**,** 125-56.

Dissanaike, S., R. Kaufman, C. D. Mack, C. Mock & E. Bulger (2008) The effect of reclined seats on mortality in motor vehicle collisions. *Journal of Trauma and Acute Care Surgery,* 64**,** 614-619.

Doud, A. N., A. A. Weaver, J. W. Talton, R. T. Barnard, J. W. Meredith, J. D. Stitzel, P. Miller & A. N. Miller (2015) Has the incidence of thoracolumbar spine injuries increased in the United States from 1998 to 2011? *Clinical Orthopaedics and Related Research,* 473**,** 297-304.

Gaewsky, J. P., A. A. Weaver, B. Koya & J. D. Stitzel (2015) Driver Injury Risk Variability in Finite Element Reconstructions of Crash Injury Research and Engineering Network (CIREN) Frontal Motor Vehicle Crashes. *Traffic Injury Prevention,* 16 Suppl 2**,** S124-31.

Golman, A. J., K. A. Danelson & J. D. Stitzel (2015) Robust human body model injury prediction in simulated side impact crashes. *Computer methods in biomechanics and biomedical engineering***,** 1-16.

Hansson, T. H., T. S. Keller & M. M. Panjabi (1987) A study of the compressive properties of lumbar vertebral trabeculae: effects of tissue characteristics. *Spine (Phila Pa 1976),* 12**,** 56-62.

Hault-Dubrulle, A., F. Robache, M. P. Pacaux & H. Morvan (2011) Determination of pre-impact occupant postures and analysis of consequences on injury outcome. Part I: a driving simulator study. *Accident Analysis & Prevention,* 43**,** 66-74.

Iraeus, J. & M. Lindquist (2016) Development and validation of a generic finite element vehicle buck model for the analysis of driver rib fractures in real life nearside oblique frontal crashes. *Accident Analysis & Prevention,* 95**,** 42-56.

Iwamoto, M., Y. Nakahira & H. Kimpara (2015) Development and Validation of the Total HUman Model for Safety (THUMS) Toward Further Understanding of Occupant Injury Mechanisms in Precrash and During Crash. *Traffic Injury Prevention,* 16 Suppl 1**,** S36-48.

Jones, D., J. Gaewsky, A. Weaver & J. Stitzel (2016a) A semi-automated approach to real world motor vehicle crash reconstruction using a generic simplified vehicle buck model. *SAE International Journal of Transportation Safety* 4**,** 267-277.

Jones, D. A., J. P. Gaewsky, M. E. Kelley, A. A. Weaver, A. N. Miller & J. D. Stitzel (2016b) Lumbar vertebrae fracture injury risk in finite element reconstruction of CIREN and NASS frontal motor vehicle crashes. *Traffic Injury Prevention,* 17 Suppl 1**,** 109-15.

Katsuhara, T., Y. Takahira, S. Hayashi, Y. Kitagawa & T. Yasuki (2017) Analysis of Driver Kinematics and Lower Thoracic Spine Injury in World Endurance Championship Race Cars during Frontal Impacts. *SAE International Journal of Transportation Safety,* 5**,** 120-132.

Kaufman, R. P., R. P. Ching, M. M. Willis, C. D. Mack, J. A. Gross & E. M. Bulger (2013) Burst fractures of the lumbar spine in frontal crashes. *Accident Analysis & Prevention,* 59**,** 153-63.

Kayanja, M. M., L. A. Ferrara & I. H. Lieberman (2004) Distribution of anterior cortical shear strain after a thoracic wedge compression fracture. *The Spine Journal,* 4**,** 76-87.

Kopperdahl, D. L. & T. M. Keaveny (1998) Yield strain behavior of trabecular bone. *Journal of Biomechanics,* 31**,** 601-8.

Miller, L., J. Gaewsky, A. Weaver, J. Stitzel & N. White. 2016. Regional Level Crash Induced Injury Metrics Implemented within THUMS v4. 01. SAE Technical Paper.

Morris, R., G. Cross & L. Bingley. 2005. Improved understanding of passenger behaviour during pre-impact events to aid smart restraint development. In *Proceedings of the 19th International Technical Conference on the Enhanced Safety of Vehilces (ESV), Washington DC, USA, June*, 6-9.

Pintar, F. A., N. Yoganandan, D. J. Maiman, M. Scarboro & R. W. Rudd. 2012. Thoracolumbar spine fractures in frontal impact crashes. In *Annu Proc Assoc Adv Automot Med.* , 277. Association for the Advancement of Automotive Medicine.

Rao, R. D., C. A. Berry, N. Yoganandan & A. Agarwal (2014) Occupant and crash characteristics in thoracic and lumbar spine injuries resulting from motor vehicle collisions. *The Spine Journal,* 14**,** 2355-2365.

SAE, S. (2007) J211-1 Instrumentation for Impact Test—Part 1—Electronic Instrumentation. *SAE International*.

Schneider, L. W., J. D. Rupp, M. Scarboro, F. Pintar, K. B. Arbogast, R. W. Rudd, M. R. Sochor, J. Stitzel, C. Sherwood & J. B. MacWilliams (2011) BioTab—a new method for analyzing and documenting injury causation in motor-vehicle crashes. *Traffic Injury Prevention,* 12**,** 256-265.

Schoell, S. L., A. A. Weaver, N. A. Vavalle & J. D. Stitzel (2015) Age-and sex-specific thorax finite element model development and simulation. *Traffic Injury Prevention,* 16**,** S57-S65.

Stemper, B. D., N. Yoganandan, J. L. Baisden, S. Umale, A. S. Shah, B. S. Shender & G. R. Paskoff (2015) Rate-dependent fracture characteristics of lumbar vertebral bodies. *Journal of the mechanical behavior of biomedical materials,* 41**,** 271-279.

Vavalle, N. A., S. L. Schoell, A. A. Weaver, J. D. Stitzel & F. S. Gayzik (2014) Application of radial basis function methods in the development of a 95th percentile male seated fea model. *Stapp Car Crash J,* 58**,** 361.

Wang, M. C., F. Pintar, N. Yoganandan & D. J. Maiman (2009) The continued burden of spine fractures after motor vehicle crashes. *Journal of neurosurgery: Spine,* 10**,** 86-92.

Ye, X., J. P. Gaewsky, B. Koya, D. A. Jones, R. Barnard, A. A. Weaver & J. D. Stitzel (2016) Automated Analysis of Driver Response in a Finite Element Crash Test Reconstruction. *Biomed Sci Instrum* Vol. 52**,** 66-74.

Ye, X., J. P. Gaewsky, L. E. Miller, D. A. Jones, M. E. Kelley, J. D. Suhey, B. Koya, A. A. Weaver & J. D. Stitzel (2018) Numerical investigation of driver lower extremity injuries in finite element frontal crash reconstruction. *Traffic Injury Prevention,* 19**,** S21-S28.

Yoganandan, N., M. W. Arun, B. D. Stemper, F. A. Pintar & D. J. Maiman (2013) Biomechanics of human thoracolumbar spinal column trauma from vertical impact loading. *Annals of advances in automotive medicine,* 57**,** 155.

Zhang, K., L. Cao, A. Fanta, M. P. Reed, M. Neal, J.-T. Wang, C.-H. Lin & J. Hu (2017) An automated method to morph finite element whole-body human models with a wide range of stature and body shape for both men and women. *Journal of Biomechanics*.

APPENDIX

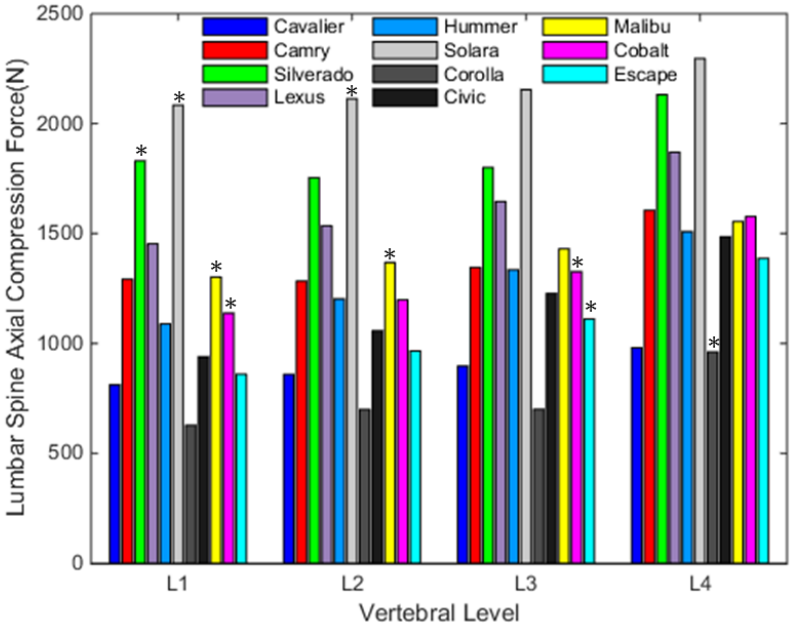

Figure A1. Lumbar spine axial compression force of 11 reconstructed baseline cases. Asterisks indicate lumbar spine fractures.

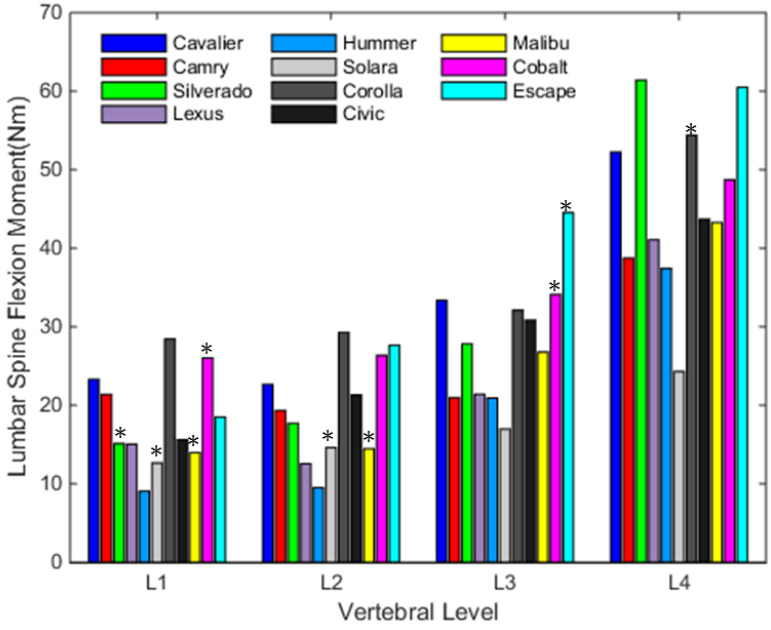

Figure A2. Lumbar spine flexion moment of 11 reconstructed baseline cases. Asterisks indicate lumbar spine fractures.